*Journal of Applied Electrochemistry* **33**: 419–429, 2003.



# Electrooxidation of methanol at platinum–ruthenium catalysts prepared from colloidal precursors: Atomic composition and temperature effects

L. DUBAU, C. COUTANCEAU, E. GARNIER, J-M. LÉGER and C. LAMY*
*Equipe Electrocatalyse, UMR 6503 CNRS – Université de Poitiers, 40 avenue du Recteur Pineau, 86 022 Poitiers cedex, France*
*(*author for correspondence, e-mail: claude.lamy@univ-poitiers.fr)*

Received 13 May 2002; accepted in revised form 24 February 2003

*Key words:* atomic composition, DMFC, electrocatalyst, methanol electrooxidation, platinum, ruthenium, temperature effect

**Abstract**

The electrocatalytic oxidation of methanol was investigated on PtRu electrodes of different atomic compositions at several temperatures (from 25 to 110 °C). Very active catalyst nanoparticles supported on active carbon (Vulcan XC 72) were obtained using the colloidal synthesis developed by Bönnemann et al. [11], allowing easy variation of the atomic composition. These electrocatalysts were characterized by TEM, EDX and XRD; results indicate that they consist of platinum nanoparticles decorated by ruthenium. Methanol oxidation was studied as a function of composition, temperature and methanol concentration. Two effects were investigated: the effect of the working temperature and the effect of the atomic composition. It appeared that for lower methanol electrooxidation overvoltages, the best catalysts are ruthenium-rich, whereas at higher overvoltages the best one is the Pt + Ru (80:20)/C composition, irrespective of the working temperature, either in half-cell or in a single DMFC.

## 1. Introduction

The electrocatalytic oxidation of methanol has been thoroughly investigated [1, 2] because methanol is a very convenient liquid fuel for fuel cells [3]. One of the key problems for development of the direct methanol fuel cell (DMFC) is the low electrochemical reactivity of methanol at low and medium temperatures, which necessitates the development of active Pt-based catalysts.

Among several bimetallic Pt–M electrocatalysts considered, Pt–Ru seems to be the most effective in terms of activity towards methanol oxidation and selectivity towards the complete oxidation to $CO_2$ [4–7].

For practical application to DMFC stacks, Pt–Ru anodes with an atomic composition of 50:50 are generally used; this is believed to be the optimum composition for methanol electrooxidation [7, 8]. However, fundamental studies have shown that the best electrocatalyst is obtained with a surface concentration close to 80% Pt–20% Ru [4, 9, 10]. The controversy about the optimum composition of Pt–Ru catalysts has not yet been resolved. Indeed, most of the fundamental studies were carried out at room temperature (~25 °C), which is far from the working temperature of a DMFC (50 to 150 °C). It is thus of interest to investigate the electrocatalytic behaviour of several Pt–Ru anodes with different composition between room and higher temperatures.

In this work, several PtRu colloid catalysts of different composition were prepared either by coreduction of platinum and ruthenium salts in order to obtain Pt–Ru alloys, or by mixing Pt and Ru colloids followed by calcination on carbon powder in order to obtain platinum decorated by ruthenium catalyst (Pt + Ru/C catalysts), or by mixing Pt/C catalyst + Ru/C powders. After physical characterization, their electrocatalytic behaviour towards methanol oxidation was first evaluated at different temperatures ranging from 20 to 50 °C in a classical electrochemical half cell. Finally, fuel cell tests were carried out at 110 °C to determine the performances of these different electrodes under the working conditions of a DMFC.

## 2. Experimental details

### 2.1. *Synthesis of the colloidal precursors of Pt–Ru catalysts*

In order to easily vary the Pt/Ru atomic ratio, a new preparation method was developed based on the synthesis of colloidal precursors using the procedure described by Bönnemann et al. [11], slightly modified.

All experiments were carried out under argon, using non hydrated salts in dry solvents. The first step consisted in the synthesis of the reducing agent by mixing a stoichiometric amount of tetraoctylammonium bromide ($Noct_4Br$) and potassium triethylhydroborate ($KBEt_3H$) in tetrahydrofuran as solvent (THF). After elimination of the precipitated KBr, a solution of tetraoctylammonium triethylhydroborate ($Noct_4BEt_3H$) was obtained which reduced the platinum or ruthenium salts according to the following reaction, written in the case of platinum as

$$PtCl_2 + 2\ Noct_4BEt_3H \rightarrow Pt[Noct_4Cl]_2 + 2\ BEt_3 + H_2$$

In this way, the platinum nanoparticles were stabilized by $Noct_4Cl$, which acts as a surfactant protecting the metal particles by its long alkyl chain. A colloidal solution of Ru particles can be obtained in the same way, as well as a colloidal solution of coreduced PtRu particles.

### 2.2. *Preparation and characterization of the methanol anode catalysts*

The colloid particles were adsorbed on Vulcan XC 72, previously treated for four hours at 400 °C under nitrogen to clean it, in order to obtain a catalyst loading of 30 wt % based on the metal content. Before using them as electrocatalysts, the organic surfactant shell of the supported colloid catalyst must be removed by a thermal treatment under air atmosphere at 300 °C. It was shown by thermogravimetric analysis that this treatment completely removes the surfactant shell without modifying the particle size. This method was used to prepare the following catalysts: Pt/XC 72; Pt–Ru/XC 72 (coreduction), Pt + Ru/XC 72, mixture of Pt/XC 72 + Ru/XC 72.

The dispersed catalyst powder was then added to a mixture of 25 wt % (based on the powder content) Nafion® solution (5 wt % from Aldrich) and ultrapure water (Millipore MilliQ – 18 MΩ cm). After ultrasonic homogenisation of the suspension, a given volume was deposited onto a fresh polished glassy carbon substrate, and the solvent was evaporated in a stream of ultrapure nitrogen at room temperature. This gave a layer (around 1 $\mu$m thickness) of catalyst with a metal loading close to 0.07 mg $cm^{-2}$.

The morphology and overall composition of the dispersed catalyst were examined by transmission electron microscopy (TEM) and EDX analysis using a Philips CM 120 microscope/EDX analyser equipped with a $LaB_6$ filament. To prepare the sample, a small drop of the suspension was put on a copper grid and the solvent was evaporated.

The crystallographic structure of the catalyst powders was investigated by X-ray diffraction (XRD). Powder X-ray diffraction patterns were recorded using a Siemens diffractometer in Bragg–Brentano geometry. Cu$K_\alpha$ X-ray radiation was used. The powder (50 mg) was deposited on a Si wafer cut along a (511) plane to reduce the background signal. The powder diffraction patterns were refined with the Powdercell software. The starting parameters were known by simulation made with the Fullprof software for a Pt–Ru alloy or a mixture of two phases (Pt and Ru).

### 2.3. *Electrochemical measurements*

The electrochemical equipment consisted of a Wenking potentiostat (model LB75), a waveform generator (Wenking VGS 72) and a X-Y-t recorder (LY1600, Linseis). The electrochemical measurements were carried out in a thermostat-controlled standard two compartment, three electrode electrochemical cell. The supporting electrolyte was 0.5 M $H_2SO_4$ (Merk, Suprapure). The counter electrode was a glassy carbon sheet. The reference electrode was a mercury/mercurous sulfate electrode (MSE) in contact with a saturated $K_2SO_4$ solution. This electrode was connected by a Luggin capillary to the working electrode compartment. All potentials are referred to that of the reversible hydrogen electrode (RHE).

The activity towards methanol oxidation of dispersed Pt–Ru electrodes with several atomic compositions ranging from 50:50 to pure platinum was evaluated by cyclic voltammetry at a very low sweep rate (1 mV $s^{-1}$) to simulate steady state conditions. Two concentrations of methanol (0.1 and 1.0 M) were used and the temperature was varied from 293 to 318 K (20 to 45 °C) by 5 °C step. The apparent activation energy was thus determined and Tafel slopes were evaluated as a function of temperature and catalyst composition.

The fuel cell tests in a single DMFC with a 5 $cm^2$ geometric surface area were carried out with a Globe Tech test bench. The $E/j$ and $P/j$ curves were recorded using a high power potentiostat (Wenking model HP 88) interfaced with a PC to apply constant current sequences and to store the data, and a variable resistance in order to fix the current applied to the cell.

Anodes for DMFC were prepared from an ink consisting of a mixture of Nafion® (5 wt % from Aldrich) solution, isopropanol and catalytic powder, brushed on a carbon gas diffusion electrode. Carbon gas diffusion electrodes were home-made using a carbon cloth from Electrochem Inc. on which was brushed an ink made of Vulcan XC 72 carbon powder and PTFE dissolved in isopropanol. The gas diffusion electrodes were loaded with 4 mg $cm^{-2}$ of a mixture of carbon powder and 15 wt % PTFE. Prior to the preparation of the membrane electrode assembly (MEA), the electrodes were heated at 150 °C to recast the Nafion® film. The metal loading of the electrodes was close to 1.5 mg $cm^{-2}$ and the Nafion® loading of the electrode was 0.8 mg $cm^{-2}$. The MEAs were prepared, by hot pressing at 130 °C for 90 s under a pressure of 35 kg $cm^{-2}$, a pretreated Nafion®117 membrane with an E-TEK cathode (2.0 mg $cm^{-2}$ Pt loading, 40% metal/C, 40% PTFE, 0.8 mg $cm^{-2}$ Nafion®) and with the home-made anodes.

## 3. Results and discussion

### 3.1. *Physicochemical characterization of Pt–Ru catalysts*

Figures 1 and 2 show TEM pictures of Pt and Pt + Ru (80:20) clusters, respectively, and Figure 3 gives the corresponding particle size distribution based on the observation made on 800 particles. The mean particle size was calculated according to the relation $\bar{d}_{\mathrm{TEM}} = (\sum n_i d_i)/n$ where $n_i$, $d_i$ and $n$ are the number, diameter of particles and the total number of particles, respectively. The mean diameter is close to 2 nm in the cases of Pt/C, Pt–Ru/C and Pt + Ru/C and close to 1.5 nm in the case of Ru/C particles. The particle size distribution is quite homogeneous. Taking the case of a Pt + Ru (80:20) catalyst as an example, the EDX analysis given in Figure 4 confirms the overall compo-

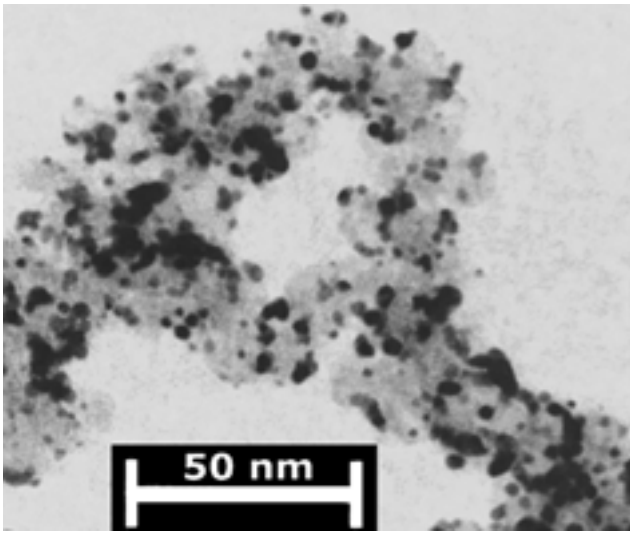


*Fig. 2.* TEM picture of a Pt + Ru (80:20) colloid catalyst supported on Vulcan XC 72.

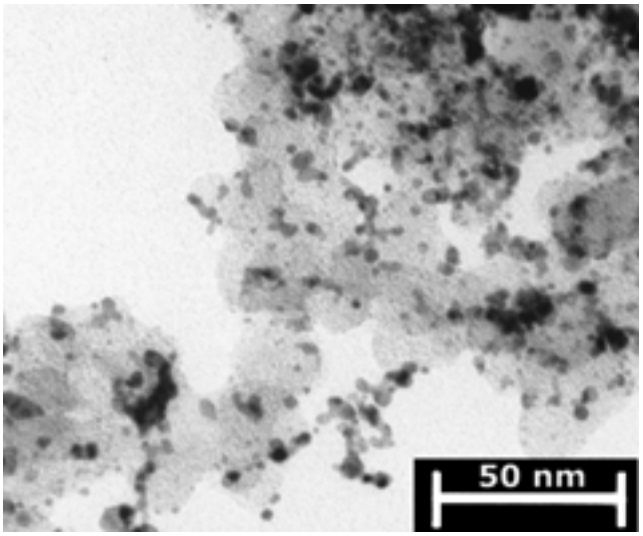


*Fig. 1.* TEM picture of a Pt colloid catalyst supported on Vulcan XC 72.

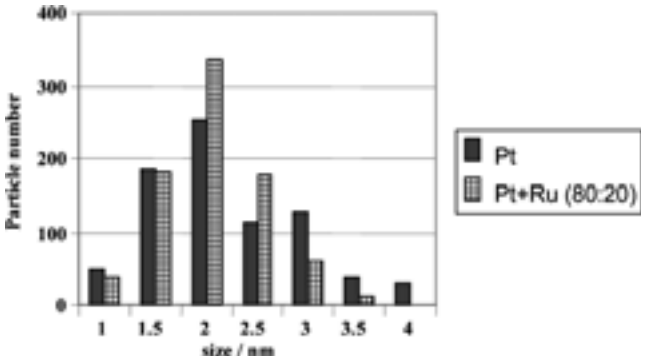


*Fig. 3.* Particle size distribution for Pt and Pt + Ru (80:20) colloid catalysts supported on Vulcan XC 72 based on the observation of 800 particles.

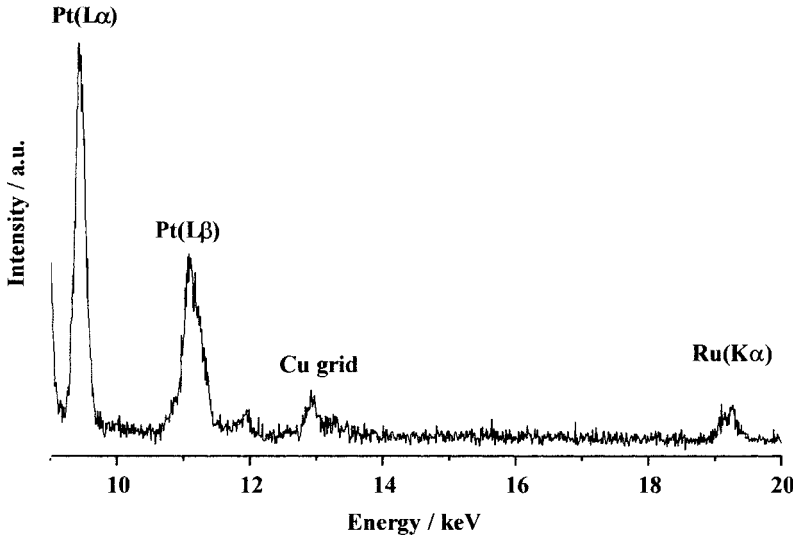


*Fig. 4.* EDX composition analysis of Pt + Ru (80:20) colloid catalyst supported on Vulcan XC 72.

sition. The Cu EDX signal is due to the copper grid where the catalyst is deposited. Only the overall composition of the catalyst is known using this analysis, not the surface composition.

Figure 5(a) and (b) show the powder X-ray diffraction patterns of the Pt + Ru (80:20) supported catalyst. This catalyst exhibits the characteristic diffraction peaks of the platinum fcc structure. But, it can also be seen in Figure 5(b) that the $2\theta$ value of diffraction peaks does not shift when we compare the Pt + Ru and the Pt catalysts. However, according to Vegard's law for a true alloy, the values of the cell parameter for bulk alloys must decrease when the ruthenium content increases. This means that the diffraction peaks must shift towards lower $2\theta$ value when ruthenium is added. Moreover, if we use the cell parameter for bulk alloys as determined by Vogel et al. [12], we should obtain as lattice parameter for the Pt–Ru (80:20) alloy $a_{\mathrm{PtRu\ (80:20)}} =$ 3.902 Å. But, the lattice parameter obtained for Pt and Pt + Ru supported catalysts was the same in both case (i.e., close to 3.923 Å) which is the lattice parameter for platinum alone. Although the ruthenium contribution is low, the shoulder corresponding to the Ru(101) peak centred close to $2\theta = 44°$, which is the most intense peak in Ru diffraction patterns, is proof of the presence of a metallic ruthenium phase. Therefore, it can be considered that in this case we are in the presence of platinum particles decorated by ruthenium particles. On the other hand, the diffractogram patterns of the coreduced Pt–Ru catalyst displays a shift of the diffraction peak towards lower $2\theta$ values when compared with platinum alone. The cell parameter of pure platinum is 3.923 Å.

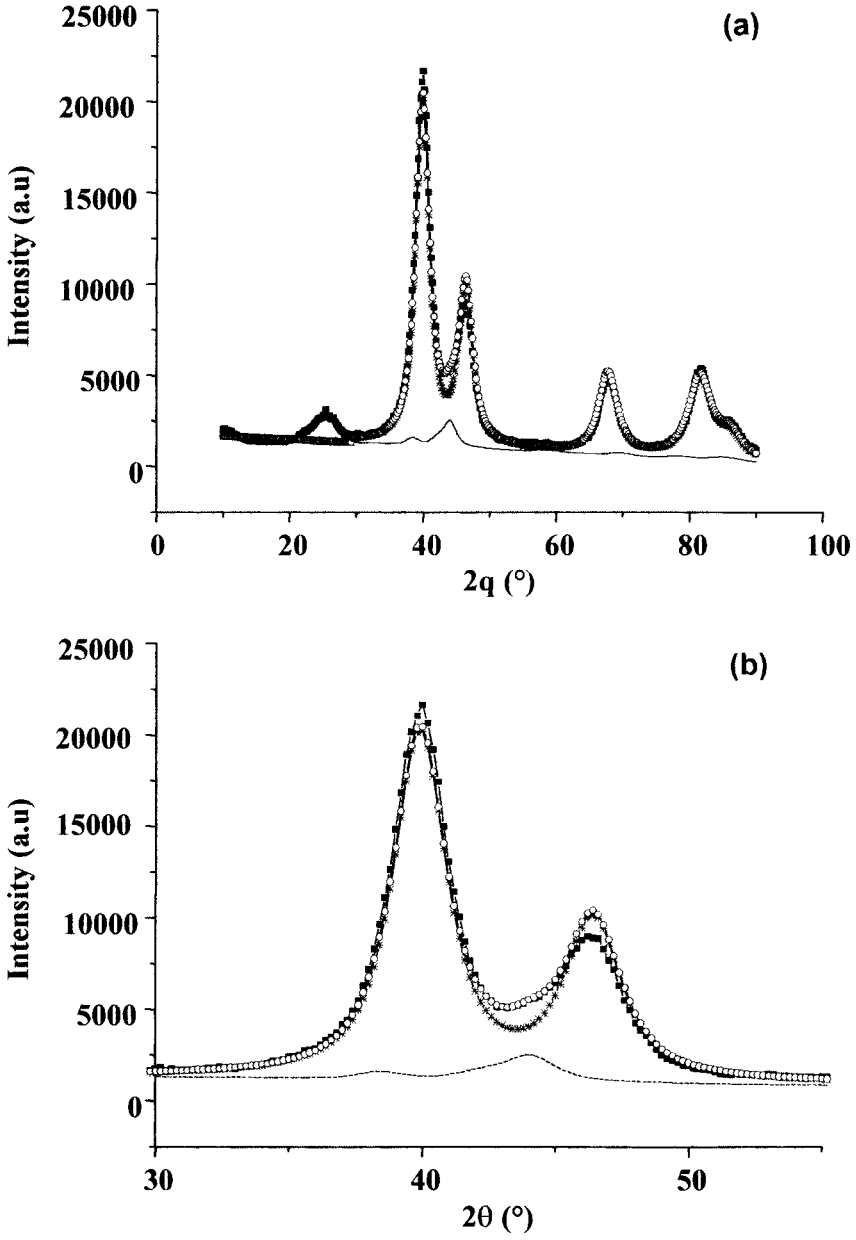


*Fig. 5.* XRD patterns of Pt + Ru (80:20) colloid catalysts supported on Vulcan XC 72. (a) Whole pattern; (b) Zoom between $2\theta = 30$ and 55°. Diffraction patterns: (■) experimental; (*) platinum; (- - - -) ruthenium; (o–o) simulation of Pt + Ru.

From the shift of the XRD peaks it is possible to calculate the new cell parameter $a_{Pt-Ru}$ from the following relation:

$$\sin\theta = \frac{(h^2 + k^2 + l^2)^{1/2}}{2a} \text{ (for a cubic stucture)}$$

We found a value of 3.905 Å for $a_{Pt-Ru}$ close to the value of 3.902 Å calculated from Vegard's law for a pure Pt–Ru (80:20) alloy. The good agreement between the theoretical and experimental values of the Pt–Ru (80:20) cell parameter shows that, in this case, we have a Pt–Ru alloy.

### 3.2. *Electrochemical measurements*

Before discussing the atomic composition effect, it is very important to determine which method of catalyst preparation leads to better performance towards methanol oxidation. As an example, Figure 6 shows the $j(E)$ curves obtained with different catalysts. It appears clearly that the best catalyst is not the alloyed one, nor the mixture of the Pt/XC 72 and Ru/XC 72 powder, but that consisting of the dispersion of Pt colloid + Ru colloid on the same carbon support, the Pt + Ru/XC 72 catalyst, that is, the platinum particles decorated by ruthenium particles. Indeed, the Pt + Ru/XC 72 leads to higher current densities for the electrooxidation of methanol than the other catalysts with the same atomic ratio for potentials lower than 0.5 V vs RHE. This result is confirmed by recent work of Waszczuk et al. [13] and Brankovic et al. [14, 15], where electrocatalytic enhancement of methanol oxidation at platinum particles decorated by ruthenium compared with alloys of the same composition and CO oxidation at ruthenium decorated by platinum compared to a commercial platinum ruthenium catalyst was demonstrated.

The effect of platinum to ruthenium atomic ratio in Pt + Ru/C catalysts is not of secondary importance. It has an effect on the rate of methanol oxidation, which can easily be seen. Figure 7 shows the cyclic voltammograms recorded in 1 M MeOH solution at 298 K on supported catalysts of different Pt/Ru atomic ratio obtained at 1 mV $s^{-1}$ between 0.00 and 0.65 V vs RHE, potential range in which the anode catalysts display a great stability and which is of great interest for the DMFC. Two effects can be related to the presence of ruthenium in the platinum based catalysts: the shift of the beginning of the oxidation wave towards lower potentials in the presence of ruthenium and especially the values of the current density – referred to the platinum mass – at a given potential which vary with the ruthenium content. To compare the behaviour of the different electrodes, the cyclic voltammetric curves were redrawn as Tafel plots $E = f(\log j)$ in order to evaluate the Tafel slopes.

Examples of the Tafel plots obtained with two different methanol concentrations (0.1 and 1.0 M) are given in Figures 8(a) and (b) and 9(a) and (b) for $T = 298$ and 318 K, respectively. At first sight, it can be seen that the Tafel slopes increase with increasing ruthenium content, irrespective of temperature and methanol concentration. In the case of pure platinum electrocatalyst, the Tafel slopes obtained are close to 80 mV $(\text{decade})^{-1}$ and 90 mV $(\text{decade})^{-1}$ at 298 and 318 K, respectively, in good agreement with previous results [16]. No change of these values with methanol concentration was observed, indicating that no significant increase in poisoning in this concentration range occurs. In the case of the Pt + Ru catalysts, the Tafel

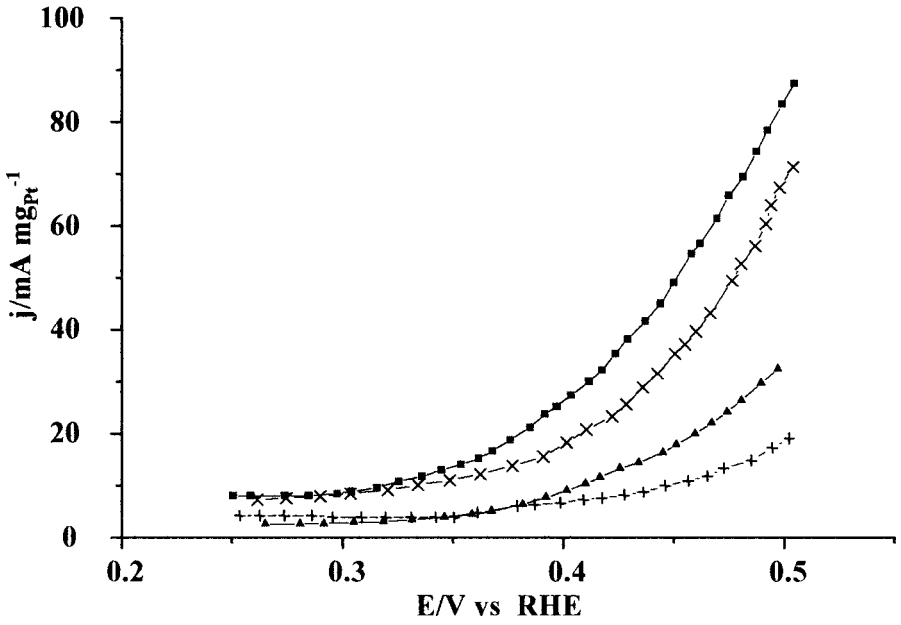


*Fig. 6.* $j(E)$ polarization curves for methanol oxidation on PtRu (80:20)/C colloid catalysts prepared in different ways (0.5 M $H_2SO_4$, 1.0 M MeOH, $v = 1$ mV $s^{-1}$, $T = 298$ K). Key: (▲) Pt/XC 72; (■) Pt + Ru/XC 72; (+) Pt/XC 72 + Ru/XC 72; (×) Pt–Ru/XC 72.

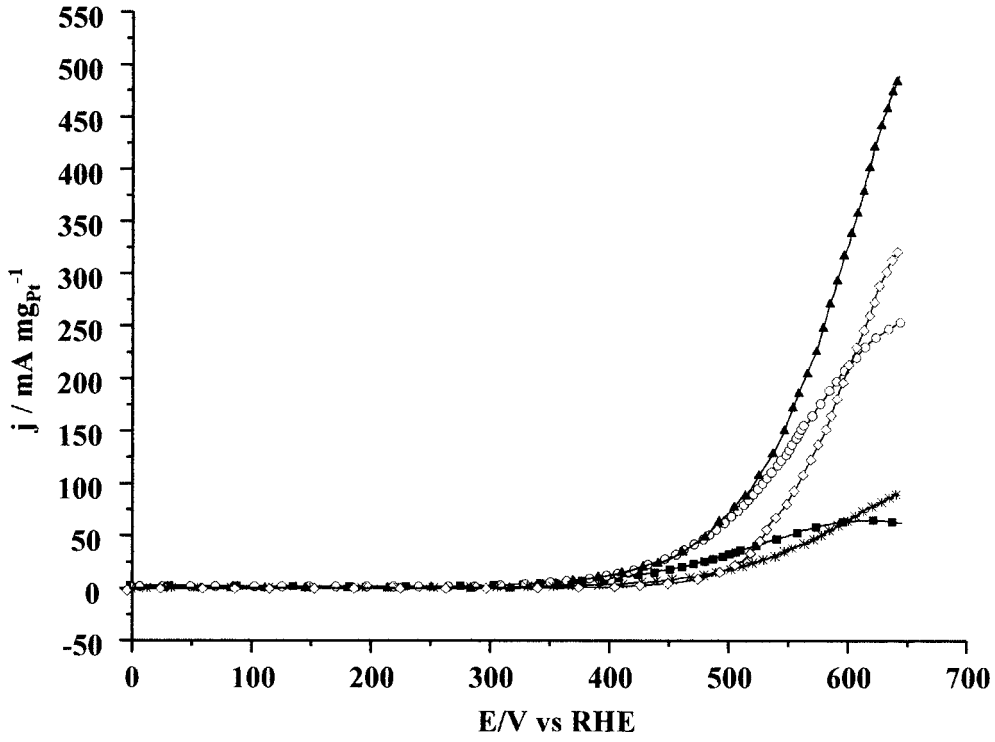


*Fig. 7.* $j(E)$ polarization curves for methanol oxidation on Pt + Ru/C colloid catalysts with different atomic compositions (0.5 M $H_2SO_4$, 1.0 M MeOH, $v = 1$ mV $s^{-1}$, $T = 298$ K). Key: (■) Pt + Ru (50:50); (○) Pt + Ru (70:30); (▲) Pt + Ru (80:20); (✳) Pt + Ru (90:10); (◇) Pt.

slopes are rather high. The values decrease when the methanol concentration increases and increase with increase in ruthenium content. Analysis of the Tafel plots give interesting results concerning the behaviour of the catalysts as a function of ruthenium content.

Considering the 1.0 molar concentration of methanol, which is close to the working condition in a fuel cell, we can see that, at 25 °C, from 0.5 V vs RHE, the Pt + Ru (80:20)/C catalyst displays a better activity than the Pt + Ru (50:50)/C one and becomes the most active catalyst at potentials higher than 0.5 V vs RHE, the Pt + Ru (50:50)/C catalyst becoming the less active one. Gasteiger et al. [17] have shown that the differences in activity as a function of the ruthenium content are due to the balance between two steps of the methanol oxidation reaction: the initial step of adsorption–dehydrogenation of methanol at platinum sites and the following step which consists in the oxidation of the adsorbed CO species at ruthenium sites. Then, the lower activity of the Pt + Ru (50:50)/C catalyst may be attributed to its lower ability for adsorption and dehydrogenation of methanol at this temperature and potential. This phenomenon is more drastic when decreasing the methanol concentration as shown in Figure 8(b). In this case, the initial adsorption–dehydrogenation step becomes the limiting step and the Pt + Ru (50:50)/C catalyst displays a weak catalytic effect compared with platinum alone. But as soon as the potential is decreased, the most active catalyst is Pt + Ru (70:30)/C, whereas the worst is Pt + Ru (90:10)/C. The Pt + Ru (50:50)/C catalyst becomes more active than the (80:20) one as shown in Figure 8(a) and (b). In this case, when the potential decreases, the kinetics of formation of oxygenated species at ruthenium is lowered and then, increasing the content of ruthenium favours the oxidation of CO species at lower potentials.

These results were confirmed by studies performed on well defined surface composition platinum–ruthenium alloys and dispersed platinum–ruthenium alloys [9, 18], where it was shown that the increase of the optimal ruthenium content leads to a decrease of the onset potential of methanol oxidation. Moreover, Iwasita et al. [19] stated that for potentials between 0.35 and 0.6 V vs RHE, the slow reaction between adsorbed CO and adsorbed OH species must be responsible for the rate of the process. They showed that the best activity towards methanol oxidation at 0.5 V vs RHE was obtained for Pt–Ru alloys with a Ru composition from 10 to 40%. In the case of ruthenium spontaneously deposited at platinum (111), the activity does not vary greatly for Ru surface coverages from 20% to 50%, with a slight enhancement for 40% of Ru coverage. On the other hand, recent work from the Wieckowski group [13, 20] showed that Pt–Ru catalysts prepared by spontaneous deposition of Ru at platinum nanoparticles displayed better activities for Ru coverage close to 40–50% at 0.3 and 0.5 V vs RHE. These results do not confirm ours. In the case of spontaneous deposition of ruthenium, the surface composition is well known because ruthenium is deposited as nanosized ruthenium islands of monoatomic height. In our case, the surface composition is not known and only the overall composition of the catalyst is known. Even if we suppose, from the XRD

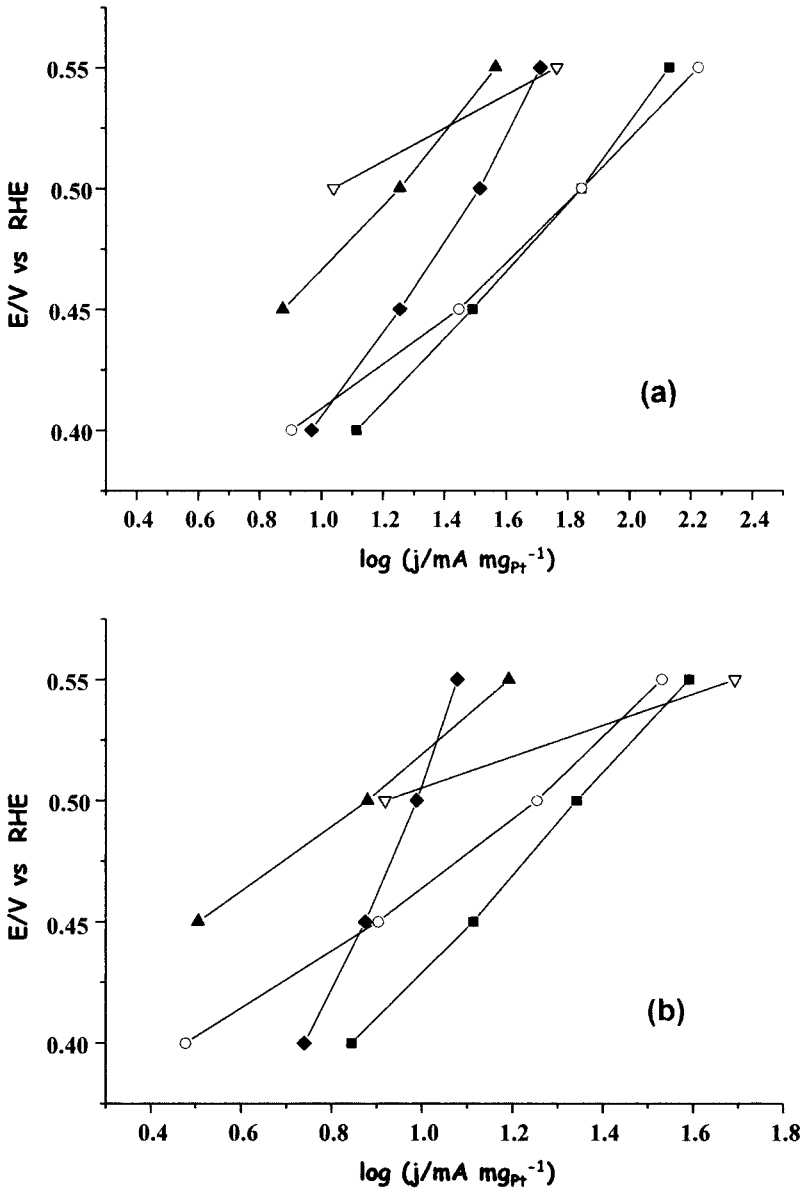


*Fig. 8.* Tafel plots for methanol oxidation on Pt + Ru/C colloid catalysts with different atomic compositions: (a) 1.0 M MeOH; (b) 0.1 M MeOH (0.5 M $H_2SO_4$, $v = 1$ mV $s^{-1}$, $T = 298$ K). Key: (◆) PtRu (50:50); (■) PtRu (70:30); (○) PtRu (80:20); (▲) PtRu (90:10); (▽) Pt.

results, that we have platinum particles decorated by ruthenium particles, we do not know the size of the platinum and ruthenium particles and then the real surface coverage. In the way our supported catalysts are prepared, it is likely that the coverage of platinum by ruthenium is higher than the value of the overall atomic composition. Therefore, for higher atomic compositions, the coverage can be higher than 50% and then the catalytic activity towards methanol oxidation decreased.

At higher temperatures (i.e., 45 °C) some changes in the electrode behaviour appear. From 0.4 to 0.5 V vs RHE, the Pt + Ru (50:50)/C catalyst displays a better activity for the oxidation of 1 M $CH_3OH$ than the Pt + Ru (80:20)/C one (Figure 9(a)), whereas at 25 °C the Pt + Ru (80:20)/C catalyst displayed a better activity than the (50:50) one from 0.42 V vs RHE (Figure 8(a)), the most active being the Pt + Ru (70:30)/C catalyst (Figure 9(a)). At potentials higher than 0.5 V vs RHE, the Pt + Ru (80:20)/C catalyst displays higher activity than the Pt + Ru (50:50)/C catalyst and at more positive potentials it tends to become more active than the Pt + Ru (70:30)/C catalyst.

To explain the enhancement with temperature of the activity of the Pt + Ru (50:50)/C catalyst compared to the Pt + Ru (80:20)/C catalyst, some authors claimed that a thermal activation of ruthenium gives it the ability to adsorb and dehydrogenate methanol at temperatures greater than 40 °C [21]. Moreover, it is well known that ruthenium allows to activate the water molecule at lower potentials than platinum, and then according to the bifunctional theory of electrocatalysis for the complete oxidation of methanol [22], the presence of large amount of ruthenium in the Pt + Ru (50:50)/C catalyst explains

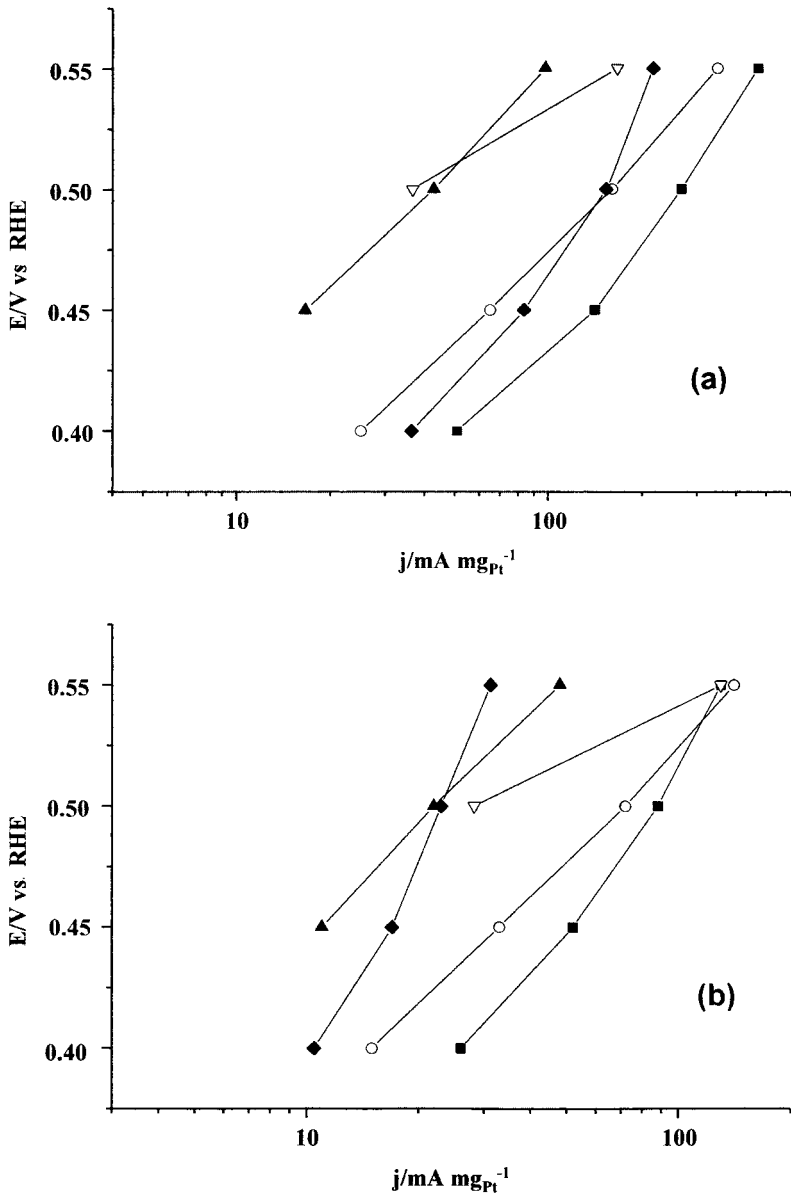


*Fig. 9.* Tafel plots for methanol oxidation on Pt + Ru/C colloid catalysts with different atomic compositions: (a) 1.0 M MeOH; (b) 0.1 M MeOH (0.5 M $H_2SO_4$, $v = 1$ mV $s^{-1}$, $T = 318$ K). Key: (◆) PtRu (50:50); (■) PtRu (70:30); (○) PtRu (80:20); (▲) PtRu (90:10); (▽) Pt.

the best activity of this catalyst compared to the ruthenium poor catalyst at lower potentials. But, at higher potentials, above 0.5 V vs RHE, platinum rich catalysts become the most active ones. According to Watanabe et al. [23] in the limiting current range, the catalytic surface is blocked by adsorbed oxygen species, which make the adsorption of organic species more difficult. Because ruthenium adsorbs oxygen species at more negative potentials, increasing the coverage with ruthenium causes the limiting current to decrease. On the other hand, according to Gasteiger et al. [9], for potentials greater than 0.5 V vs RHE in the temperature range 25 to 60 °C, pure platinum displays a greater activity than ruthenium for methanol oxidation. The combination of both effects explains the decrease in limiting current with an increase of the ruthenium atomic ratio.

From these results, it can be underlined that:

(i) at a given constant potential lower than 0.5 V vs RHE, increasing the temperature requires an increase in the ruthenium content to enhance the rate of methanol oxidation.

(ii) at a given constant potential greater than 0.5 V vs RHE, increasing the temperature requires a decrease in the ruthenium content to enhance the rate of methanol oxidation.

A slight increase in the operating temperature greatly enhances the reaction kinetics of methanol oxidation, increasing the current densities greatly. Figure 10 shows the increase with temperature of the oxidation current densities of methanol on the supported Pt + Ru (80:20)/C catalyst recorded at 1 mV $s^{-1}$ in a 0.5 M $H_2SO_4$ + 1.0 M $CH_3OH$ solution. From these curves, log $j/T^{-1}$ Arrhenius plots were drawn for different

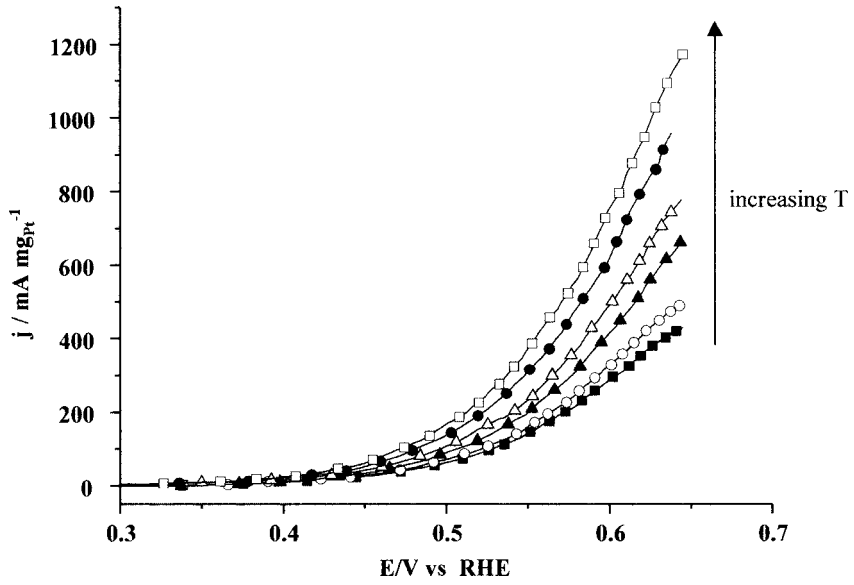


*Fig. 10.* $j(E)$ polarization curves for methanol oxidation on a Pt + Ru (80:20)/C colloid catalyst at different temperatures (0.5 M $H_2SO_4$, 1.0 M MeOH, $v = 1$ mV $s^{-1}$). Key: (■) 293, (○) 298, (▲) 303, (△) 308, (●) 313 and (□) 318 K.

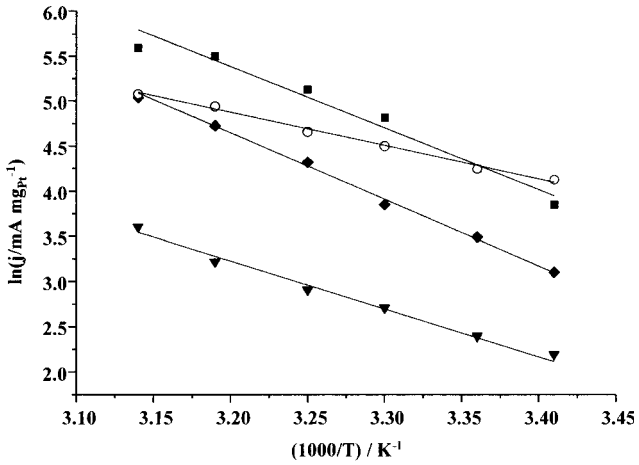


*Fig. 11.* Arrhenius plots obtained at 0.5 V on Pt + Ru/C colloid catalysts with different atomic compositions (0.5 M $H_2SO_4$, 1.0 M MeOH, $v = 1$ mV $s^{-1}$). Key: (♦) Pt + Ru (50:50)/C; (■) Pt + Ru (70:30)/C; (○) Pt + Ru (80:20)/C; (▼) Pt/C.

catalyst compositions as shown in Figure 11, the slopes of which allow determination of the apparent activation energy $\Delta H^*$. At 0.5 V vs RHE, the values of the apparent activation energy are 60 kJ $mol^{-1}$ for the Pt + Ru (50:50) and Pt + Ru (70:30) catalysts, 30 kJ $mol^{-1}$ for the Pt + Ru (80:20) catalyst and an intermediate value of 45 kJ $mol^{-1}$ for the Pt catalyst. Such values agree well with those obtained by Gasteiger et al. [9] on polycrystalline Pt–Ru alloys of different atomic compositions.

For electrocatalysts with high ruthenium content, the limiting step may be the adsorption–dehydrogenation of methanol, as suggested by some results from i.r. studies where it was shown that on ruthenium-rich surface, the covering by CO adsorbed species is small [4]. Therefore a value of the apparent energy of activation close to 60 kJ $mol^{-1}$ is reasonable. For ruthenium-poor catalyst, the low value of the apparent energy of activation (30 kJ $mol^{-1}$) cannot be attributed to the limiting step generally admitted for platinum rich catalyst, that is, the oxidation of adsorbed CO species, but rather to the CO surface diffusion from platinum sites towards ruthenium sites where the oxygenated species on Ru oxidize the CO species [9]. Finally the value for the platinum catalyst (45 kJ $mol^{-1}$) may be attributed to the oxidation of $CO_{ads}$ to $CO_2$, which is the rate determining step, according to the following equation:

$$CO_{ads} + OH_{ads} \rightarrow CO_2 + H^+ + e^-$$

### 3.3. *Electrochemical behaviour in a DMFC*

These temperature studies were extended from 50 to 110 °C using a single DMFC with a 5 $cm^2$ surface area electrode. The cell voltage ($E$) and power density ($P$) against current density ($j$) curves were recorded at 50, 70, 90, 100, 110 °C, on Pt + Ru/C electrodes with three atomic ratios (80:20; 70:30; 50:50) using the colloid catalyst particles synthesized in this work. For example, Figure 12 shows the performances of a Pt + Ru (70:30)/C electrode at different temperatures. It appears clearly that increasing the temperature greatly increases the performance of the cell, from a maximum power density of 30 mW $cm^{-2}$ at 50 °C to 110 mW $cm^{-2}$ at 110 °C, almost four times higher. This fact confirms the difficulty of oxidizing methanol at low temperatures and the necessity to work at temperatures higher than 100 °C to enhance the electrode kinetics and, thus, the performance of a DMFC.

If we compare the single DMFC performances of three anodes with different Pt/Ru compositions, we see a similar behaviour as that obtained at lower temperatures.

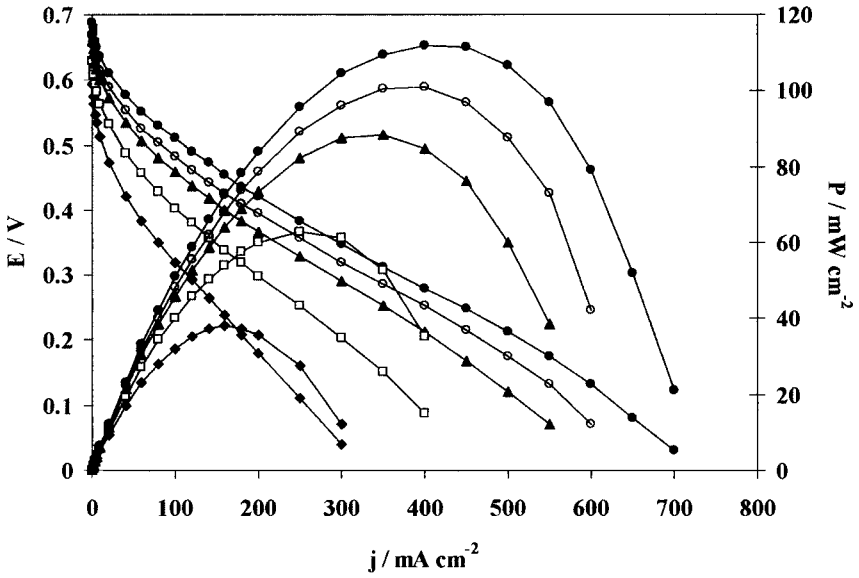


*Fig. 12.* Cell voltage ($E$) and power density ($P$) against current density ($j$) curves recorded in a single DMFC using a Pt + Ru (70:30)/C anode of 5 $cm^2$ surface area, at different temperatures (cathode E-TEK, Nafion®117 membrane, $P_{CH_3OH} = 3$ bar, $P_{O_2} = 3.5$ bar). Key: (♦) 50, (□) 70, (▲) 90, (○) 100 and (●) 110 °C.

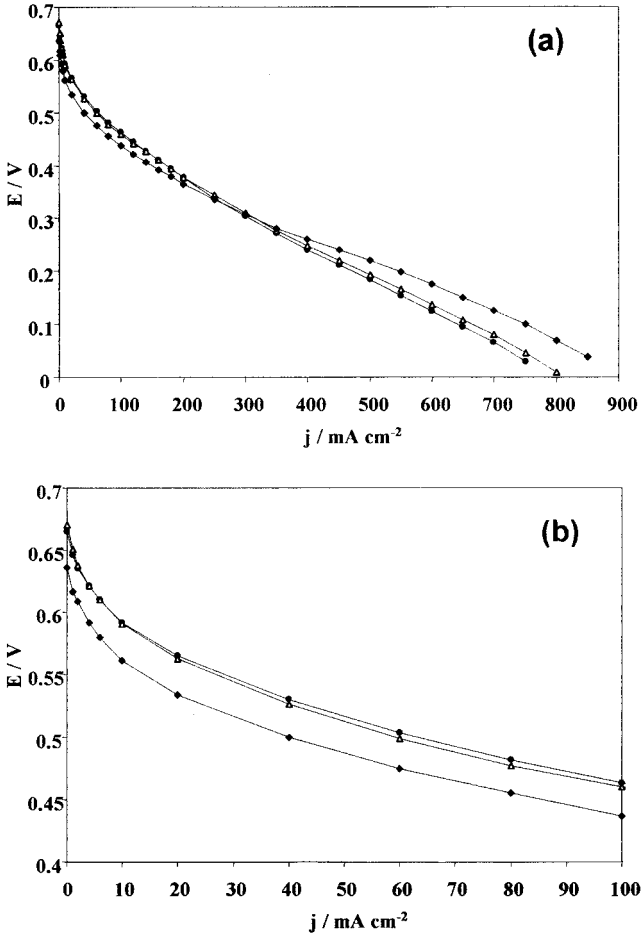


*Fig. 13.* Cell voltage ($E$) against current density ($j$) curves recorded in a single DMFC using Pt + Ru/C anodes of different compositions with a 5 $cm^2$ surface area, at 110 °C (cathode E-TEK, Nafion®117 membrane, $P_{CH_3OH} = 1.9$ bar, $P_{O_2} = 2.5$ bar). (a) Whole curves, (b) zoom between $j = 0$ and $j = 100$ mA $cm^{-2}$. Key: (●) Pt + Ru/C (50:50); (△) Pt + Ru/C (70:30); (♦) Pt + Ru/C (80:20).

Indeed, Figure 13 shows the $E(j)$ curves recorded at 110 °C with different compositions of Pt/Ru anodes, all other parameters being the same. It appears that at higher cell voltages (i.e., from 0.7 to 0.35 V) the Pt + Ru (50:50)/C catalyst gives the best performance since higher current densities are obtained at higher cell potentials (lower anode potentials), the lowest performances being reached by the ruthenium poor catalyst. But, at cell voltages lower than 0.35 V (i.e., at higher overvoltages with respect to anodic oxidation of methanol) the (80:20) ruthenium poor catalyst becomes the most active catalyst since it gives higher power densities. This fact was confirmed in our laboratory at electrochemically prepared catalysts with different Pt/Ru ratios. In this case, the catalyst was a true alloy of platinum and ruthenium and, in a DMFC, we again obtained a better activity at higher cell voltages for Pt–Ru (50:50)/C catalyst compared to Pt–Ru (65:35)/C and Pt–Ru (80:20)/C catalysts, and a better activity at lower cell voltages for the (80:20) one [24].

## 4. Conclusion

The goal of this work was to obtain results to answer to the following questions. What is the best composition of Pt/Ru catalysts for the electrooxidation of methanol? Does this optimal composition depends on temperature? The results obtained here do not lead to a definitive conclusion about the best catalyst composition for methanol electrooxidation. However, they show clearly that the structure and composition of the catalyst are very important, that the catalytic activity varies drastically with the Pt/Ru ratio, and that temperature has an important effect on the catalytic activity by activation of the ruthenium sites which allowed this metal to adsorb–

dehydrogenate methanol at temperatures higher than 40 °C.

Concerning the structure of the catalyst, we have shown that, in agreement with recent results [13], platinum particles decorated with ruthenium display higher activity towards methanol oxidation than alloyed particles of the same atomic composition. The best composition of Pt + Ru/C catalysts depends greatly on the working potential. This fact can be related to the change in the rate-determining step as a function of the potential. At lower potentials for methanol oxidation, the rate-determining step is the activation of water, and the oxidation of CO species to $CO_2$ [19], and then, a high content of ruthenium is needed to enhance the electroactivity; at higher potentials, adsorption–dehydrogenation of methanol becomes the rate determining step due to the presence of adsorbed oxygen species [23], and then, platinum rich catalysts are better.

For practical applications, the activity of catalysts must be discussed in the potential region up to 0.5 V vs RHE in order to obtain acceptable cell voltages for the DMFC. In this case, the best catalyst for methanol oxidation at high temperatures (80 to 120 °C) is a ruthenium rich catalyst. At this anode potential of 0.5 V corresponds a cell voltage of the DMFC close to 0.4 V considering the cathode potential close to 0.8–0.9 V vs RHE [25, 26]. But, it is also interesting to have some data on methanol oxidation catalysts at potentials higher than 0.5 V vs RHE, up to 0.6 V vs RHE.

## References


1. C. Lamy and J-M. Léger, *in* A. Wieckowski (Ed), 'Interfacial Electrochemistry, Theory, Experiments and Applications' (Marcel Dekker, New York, 1999), chapter 48, pp. 885–894.
2. S. Wasmus and A. Küver, *J. Electroanal. Chem.* **461** (1999) 14.
3. K.V. Kordesh and G.R. Simader, *Chem. Rev.* **95** (1995) 191.
4. A. Kabbabi, R. Faure, R. Durand, B. Beden, F. Hahn, J-M. Léger and C. Lamy, *J. Electroanal. Chem.* **444** (1998) 41.
5. T.J. Shmidt, H.A. Gasteiger and R.J. Behm, *Electrochem. Com.* **1** (1999) 1.
6. A. Hamnett, *in* A. Wieckowski (Ed), 'Interfacial Electrochemistry, Theory, Experiments and Applications' (Marcel Dekker, New York, 1999), chapter 47, pp. 843–883.
7. H.N. Dinh, X. Ren, F.H. Garzon, P. Zelenay and S. Gottesfeld, *J. Electroanal. Chem.* **491** (2000) 222.
8. M. Watanabe, M. Uchida and S. Motoo, *J. Electroanal. Chem.* **229** (1987) 395.
9. H.A. Gasteiger, N. Markovic, P.N. Ross and E.J. Cairns, *J. Electrochem. Soc.* **141** (1994) 1795.
10. R. Ianello, V.M. Schmidt, U. Stmming, J. Stumper and A. Wallau, *Electrochim. Acta* **39** (1994) 1863.
11. H. Bönnemann, W. Brijoux, R. Brinkmann, E. Dinjus, T. Joussen and B. Korall, *Angew. Chem. Int. Engl.* **30** (1991) 1312.
12. W. Vogel, P. Britz, H. Bönnemann, J. Rothe and J. Hormes, *J. Phys. Chem. B* **101** (1997) 11029.
13. P. Waszczuk, J. Solla-Gullón, H.-S. Kim, Y-Y. Tong, V. Montiel, A. Aldaz and A. Wieckowski, *J. Catal.* **203** (2001) 1.
14. S.R. Brankovic, J-X. Wang, Y. Zhu, R. Sabatini, J. McBreen and R.R. Adzic, *J. Electroanal. Chem.* **524–525** (2002) 231.
15. S.R. Brankovic, N.S. Marinkovic, J-X. Wang and R.R. Adzic, *J. Electroanal. Chem.* **532** (2002) 57.
16. F. Gloaguen, T. Napporn, M-J. Croissant, J.-M. Léger, C. Lamy and S. Srinivasan, *in* J. McBreen, S. Mukerjee and S. Srinivasan (Eds), Proceedings of the Symposium on 'Electrode Materials and Processes for Energy Conversion and Storage IV', **PV 97–13** (The Electrochemical Society, Pennington, NJ, 1997), pp. 131–138.
17. H.A. Gasteiger, N. Markovic, P.N. Ross and E.J. Cairns, *J. Phys. Chem.* **97** (1993) 12020.
18. J. Goodenough and R. Manoharan, *Chem. Mater.* **1** (1989) 391.
19. T. Iwasita, H. Hoster, A. John-Anaker, W.F. Lin and W. Vielstich, *Langmuir* **16** (2000) 522.
20. Y.Y. Tong, H.S. Kim, P.K. Babu, P. Waszczuk, A. Wieckowski and E. Olfield, *J. Am. Chem. Soc.* **124**(3) (2002) 468.
21. D. Chu and S. Gilman, *J. Electrochem. Soc.* **143** (1996) 5.
22. M. Watanabe and S. Motoo, *J. Electroanal. Chem.* **60** (1975) 275.
23. M. Watanabe and S. Motoo, *J. Electroanal. Chem.* **60** (1975) 267.
24. C. Coutanceau, A. Rakotondrainibe, E. Garnier, S. Pronier, J.-M. Léger and C. Lamy, submitted to *J. Appl. Electrochem.*
25. M.K. Ravikumar and A.K. Shukla, *J. Electrochem. Soc.* **143** (1996) 2601.
26. X. Ren, T.E. Springer and S. Gottesfeld, *J. Electrochem. Soc.* **147** (2000) 92.